Atmos. Meas. Tech. Discuss., 4, 7211–7240, 2011
www.atmos-meas-tech-discuss.net/4/7211/2011/
doi:10.5194/amtd-4-7211-2011

Atmospheric Measurement Techniques Discussions

Influence of aerosol and surface reflectance variability on hyperspectral observed radiance

C. Bassani[1], **R. M. Cavalli**[1], **and P. Antonelli**[2]

[1]Institute for Atmospheric Pollution Research (IIA) – Italian National Research Council (CNR), Via Salaria Km. 29,300 – 00015 Monterotondo, Rome, Italy
[2]Space Science Engineering Center, University of Wisconsin, Madison, USA

Received: 1 October 2011 – Accepted: 25 October 2011 – Published: 5 December 2011

Correspondence to: C. Bassani (cristiana.bassani@iia.cnr.it)

Published by Copernicus Publications on behalf of the European Geosciences Union.

Abstract

Physically based retrievals of aerosol properties from remotely sensed data usually requires extensive assumptions on particulate type and vertical distribution, and ground surface reflectivity. New satellite missions, based on high spectral resolution instruments, such as PRISMA (Hyperspectral Precursor and Application Mission), represent a valuable opportunity to mitigate the dependency of the retrieval accuracy from the such (a-priori) information. This paper aims to address the potential of these new observing systems in retrieving aerosol properties specifically over coastal areas. Goal has been achieved by using simulated radiances obtained combining two aerosol models (urban and continental), and two reflecting surfaces, dark (water) and bright (sand) for the PRISMA instrument. Results showed that, in the continental regime, the expected instrument sensitivity would allow for retrieval accuracy of the optical thickness at 550 nm of 0.02 or better, with a dark surface surrounded by dark areas. Study also showed that for the urban regime, the surface plays a more significant role, with a bright surface surrounded by dark areas providing the best conditions for the aerosol load retrievals, and dark surfaces representing less suitable situations for accurate retrievals independently of the surroundings. Moreover the results obtained, led the authors to the conclusions that high resolution observations of Earth spectrum between 400 and 1000 nm, through the use of a physically based inversion system, would allow for a significant improvement of the retrieval accuracy for anthropogenic/natural aerosol, over coastal regions.

1 Introduction

Aerosols play a significant role in atmospheric radiative forcing by scattering and absorbing radiation and by modifying physical and radiative properties of clouds (IPCC, 2001, 2007). Despite the improvements in knowledge about aerosol forcing, a great deal remains uncertain. Significant effort is being made to infer the properties of

AMTD
4, 7211–7240, 2011

aerosol at regional and global scale by the use of data from passive airborne and space-borne observing systems. An overview of the aerosol retrieval algorithms developed for passive space-borne sensors is presented in King et al. (1999). However the implementation of these strategies led to operational algorithms which provide a variety of results. Recent inter-comparisons of aerosol retrievals obtained over land by different algorithms, presented in Kokhanovsky et al. (2007), has shown relatively large discrepancies between different satellite observations. Furthermore, it was shown that the methodologies used for aerosol retrieval from multispectral data, were heavily dependent on the characterization of the a-priori knowledge on aerosol models and ground surface properties.

For example, the algorithms used to determine aerosol properties over land and over ocean based on EOS-MODIS (both Terra and Aqua satellites) observed radiances, assumes that surface reflectances in the visible and near infrared are correlated (Kaufman et al., 1997c, 2002).

The challenge of imaging spectroscopy, hereafter referred to as hyperspectral remote sensing, is to mitigate the dependency of current aerosol retrieval algorithms from these kind of assumptions, by providing observations at higher spectral and spatial resolution (Guanter et al., 2009; Gao et al., 2009; Goetz et al., 1985). However having a single instrument in orbit represents a limitation in data availability which translates in lack of opportunities for hyperspectral-based algorithm development and validation.

Currently, high spectral resolution data are acquired by the Compact High-Resolution Imaging Spectrometer (CHRIS) as part of the Project for On-Board Autonomy (PROBA) platform system (Barnsley et al., 2004). In addition, two new hyperspectral missions namely: EnMAP (Environmental Mapping and Analysis Program) (Kaufmann et al., 2008), and PRISMA (Hyperspectral Precursor and Application Mission) (Galeazzi et al., 2008), have started. Both missions are intended to provide new observations at approximately 30 m resolution to test and improve the algorithms currently used in atmospheric studies.

AMTD
4, 7211–7240, 2011

Extensive literature on the results obtained from simulated hyperspectral data exists (Kaufman et al., 1997a; Vermote et al., 1997; Kotchenova et al., 2008; Kokhanovsky et al., 2010). In particular Guanter et al. (2007); Gao et al. (2009); Bassani et al. (2010) showed that with hyperspectral data, minimization algorithms can be used to solve the inverse problem to infer the aerosol optical thickness for a given aerosol model. However also for these studies a-priori assumption on the aerosol model can yield to inaccurate characterization of the atmospheric radiative field, which is dependent on the phase function of the aerosol.

For this reason, the aim of this study is to investigate the influence of the aerosol model and of the surface on hyperspectral observations, with the goal of improving the robustness of the inversion algorithms. Part of the investigation was based on an ideal instrument with 2.5 nm spectral resolution and part on PRISMA-like data obtained convolving the ideal instrument data with an instrument response function with Full Width at Half Maximum (FWHM $\leq$ 10 nm) and spectral coverage between 400–1000 nm.

The particular aerosol properties considered in this study are aerosol loading at optical thickness of 550 nm, referred to as τ_{550}, and the aerosol model used (urban or continental). The analysis was performed on dark and bright surfaces to evaluate the radiative impact of the reflective characteristics of the target areas and the surrounding environment on the observed radiances. Synthetic radiances were simulated using the forward model 6SV1 (Second Simulation of a Satellite Signal in the Solar Spectrum – Vector) (Vermote et al., 2006).

Specific goals of the presented study along with followed methodology are described in detail in Sect. 2, while Sect. 3 contains the general results obtained for an idealized hyperspectral instrument, and Sect. 4 focuses on the specific results obtained for a PRISMA-like instrument. Final conclusions are left to the closing section.

AMTD
4, 7211–7240, 2011

2 Methodology

This section aims to introduce the goals of the presented study, and the scientific methodology followed for their achievement.

The first goal is to provide qualitative analysis of how observed radiance depend on optical thickness τ_{550} at 500 nm, on aerosol models over land (continental and urban), and on target surface reflective properties (including target surroundings). Analysis was based on simulated radiances at 2.5 nm resolution for the spectral region of 400–2500 nm. This part is mostly theoretical and therefore intentionally general (not linked to existing and/or future instruments).

The second goal is to identify optimal conditions, in terms of target surface reflective characteristics (including surrounding areas), for anthropogenic/natural aerosol property retrievals over coastal regions. For this part simulated data are tailored to PRISMA instrument specification with FWHM $\leq$ 10 and spectral coverage between 400–1000 nm. The goal was achieved by comparing the sensitivity of the observed (simulated) radiances to incremental changes in aerosol optical thickness of 0.02, with the signal to noise ratio specified for the PRISMA instrument, for different target areas.

In both cases the study takes explicitly in consideration the adjacency effect, i.e. the impact of the surroundings of the target area on the observed radiances. The remaining part of this section is divided in four subsections, the first being dedicated to the theoretical aspects of the simulated of observed radiances for an ideal instrument; the second being focused to the contribution of the aerosol loading and models on the simulated data; the third one being dedicated to the surface contribution to the simulated radiances; and the last one describing how the simulated data for the ideal instrument were convolved to generate PRISMA-like observations.

2.1 Observation simulation

Synthetic radiances used for this study, were generated within the spectral domain of 400–2500 nm sample at 2.5 nm, for different values of aerosol optical thickness at

AMTD
4, 7211–7240, 2011

550 nm, τ_{550}, and for urban, and continental models. The approach used in the simulation is based on the equation for top of the atmosphere radiance presented in Vermote et al. (1997), which considers negligible the anisotropy of the reflecting surface, that is it assumes a Lambertian surface:

$$L_v(\lambda) = \frac{\mu_s E_s(\lambda)}{\pi} t^g(\lambda) \left[\rho^{atm}(\lambda) + \frac{T^{\uparrow}(\lambda) T^{\downarrow}(\lambda) \rho_{gnd}(\lambda)}{1 - S(\lambda)\rho_{gnd}(\lambda)} \right] \quad (1)$$

where $L_v(\lambda)$ is the radiance by the ideal sensor within the considered Field Of View (FOV); $E_s(\lambda)$ is the solar irradiance at the Top Of Atmosphere (TOA); $t^g(\lambda)$ is the transmittance due to gaseous absorption; $\rho^{atm}(\lambda)$ is the intrinsic atmospheric reflectance; $T^{\uparrow}(\lambda) = e^{-\tau(\lambda)/\mu_v} + t_d(\mu_v, \lambda)$ and $T^{\downarrow}(\lambda) = e^{-\tau(\lambda)/\mu_s} + t_d(\mu_s, \lambda)$ are the total upwelling and downwelling transmittance, both with direct, $e^{-\tau(\lambda)/\mu_{s,v}}$, and diffuse, $t_d(\mu_{s,v}, \lambda)$, components; $\mu_{s,v} = \cos(\theta_{s,v})$ where $\theta_{s,v}$ are the solar, "s", and view, "v", zenith angle; $\tau(\lambda)$ is the atmospheric optical thickness; $S(\lambda)$ is the atmospheric spherical albedo, defined in Kokhanovsky (2008), and $\rho_{gnd}(\lambda)$ is the at-ground surface reflectance.

Simulated radiances were obtained through the straightforward application of Eq. (1) using the last version (v. 6SV1, Kotchenova et al., 2008) of the Second Simulation of a Satellite Signal in the Solar Spectrum (6S) radiative transfer code (Vermote et al., 1997). The 6SV1 is an open-source code which shows significant improvements with respect to previous versions as described in Vermote and Kotchenova (2009).

Simulation of the radiance observed by the ideal instrument were obtained accounting not only for the radiative contribution of the viewed target, but also for the contribution of areas surrounding the target FOV (Field Of View) (mainly due to scattering processes). This second contribution is generally referred to as the adjacency effect. The equation used to calculate the observed radiance which accounts for the environmental contribution was presented by (Vermote et al., 1997):

AMTD
4, 7211–7240, 2011

$$L(\lambda) = \frac{\mu_s E_s(\lambda)}{\pi} t^g(\lambda) \left[\rho^{atm}(\lambda) + \frac{T^{\uparrow}(\lambda) e^{-\tau/\mu_v} \rho_{gnd}(\lambda) + T^{\uparrow}(\lambda) t_d(\mu_v) < \rho_{gnd}(\lambda) >}{1 - S(\lambda) < \rho_{gnd}(\lambda) >} \right] \quad (2)$$

where $L(\lambda)$ is the total observed radiance coming from the considered FOV and its surroundings, and $< \rho_{gnd}(\lambda) >$ represents the mean of the environmental reflectance around the viewed target. When the neighboring targets are equal to the viewed target ($< \rho_{gnd}(\lambda) > = \rho_{gnd}(\lambda)$) Eqs. (2) and (1) become identical.

2.2 Aerosol contribution

Aerosol contribution to observed radiances is mostly determined by the radiation extinction due to scattering and absorption. Aerosol loading is a primary quantity in driving radiation extinction, and it is generally parametrized by the optical thickness at 550 nm, referred to as τ_{550}. The sensitivity study presented in this paper is based on radiances simulated for:

- $\tau_{550} \in \{0.00 - 2.00\}$ at intervals of $\Delta\tau_{550} = 0.02$. The increment $\Delta\tau_{550}$ was set to 0.02 to allow for direct calculation of the radiance gradient $\frac{\Delta L}{\Delta\tau_{550}}$ with the same accuracy level of in-situ observation provided by sun sky-radiometer, as CIMEL (Holben et al., 1998), generally used for the validation of the remote aerosol retrievals. It is worth mentioning that also aerosol retrievals provided by MODIS have a comparable accuracy of $\Delta\tau \approx 0.03 - 0.05$ as described in Kaufman et al. (1997b). Range of optical thicknesses used in the simulation was the widest allowed by 6SV1. Furthermore, it is the same range used to generate the main-group elements for τ_{550} in the retrieval algorithm applied to hyperspectral remotely data (Guanter et al., 2007; Bassani et al., 2010). Values of τ_{550} outside of this domain must be treated with different atmospheric radiative transfer codes, as in the L-POM model presented in Alakian et al. (2008), which enables the simulation of the radiative field in very high aerosol loading conditions.

AMTD
4, 7211–7240, 2011

– Both urban and continental aerosol models to verify the role of the aerosol model in the direct and diffuse components of the solar beam during its propagation through the atmosphere in coastal environment. The other aerosol properties which are relevant to atmospheric radiative transfer modeling are all defined by the aerosol model. The present study focuses on the two models which are mostly used in remote data acquired "over land". Both models combine the four basic components: sea-salt, water-soluble, soot and dust-like (Lenoble, 1985; d'Almeida et al., 1991; Kokhanovsky, 2008; Vermote et al., 2006). Table 1 shows the volumetric percentage of the basic components for the urban and continental aerosol regimes, as contained in the source code 6SV1.

2.3 Surface contribution

To properly simulate observed radiances for the presented study the influence the surface contributions was explicitly taken into consideration. The interaction between the radiation and the surface affects both the direct and diffuse components coming off the viewed target and the diffuse component from adjacent targets which is, successively, scattered from the atmospheric aerosols.

Simulation of observed radiances, generated for this study, satisfies the Lambertian condition, required by Eqs. (1) and (2), and also must be representative of coastal regions (areas of interest). Therefore the $\rho_{\mathrm{gnd}}(\lambda)$, in order to satisfy the previous requirements, were selected for sand (bright surface) and water (dark surface). Figure 1 shows the two reflectance spectra used by 6SV1 for the analysis. The two spectral signature were used for the viewed and adjacent target. Table 2 provides the naming convention for the radiance generated by combining the two spectral signatures for the viewed and adjacent targets.

AMTD
4, 7211–7240, 2011

2.4 PRISMA

PRISMA (PRecursore IperSpettrale della Missione Applicativa) is a medium-resolution hyperspectral imaging instrument developed under the guidance of the Italian Space Agency (ASI) (Galeazzi et al., 2008). Instrument specifications are listed in Table 3. While the first part of the presented study is focused on the sensitivity of an ideal hyperspectral sensor, the second part aims to investigate in detail the potential use of PRISMA for aerosolic retrievals in coastal regions and to demonstrate limits and benefits of the adjacency effect. Radiances simulated according to Sects. 2.1, 2.2, and 2.3, in the 400–2500 nm were convolved to the response function of the PRISMA channels belonging to the spectral domain where the aerosol effects are relevant, that is 400–1000 nm. From the Table 3, all the 92 channels of the first spectrometer fall into this spectral domain.

To assess the value of PRISMA in retrieving aerosol loadings, the ratio $\frac{L(\lambda)}{\Delta L(\lambda)}|_{\tau_{550}}$, where $\Delta L(\lambda)$ is the variation of radiance due to a 0.02 increment in aerosol optical thickness, was compared to the minimum Signal to Noise Ratio (SNR $\approx$ 200) specified for the instrument and listed in Table 3. Cases (combinations of aerosol and surface contributions) associated to $\frac{L(\lambda)}{\Delta L(\lambda)}|_{\tau_{550}} < 200$ were considered invertible by PRISMA-tailored retrieval algorithm.

3 General results for idealized intrument

This section shows the results obtained by investigating the dependency of the observation simulated according to Sects. 2.1, 2.2, and 2.3 on different combination of aerosol and surface properties. The geometrical conditions used in the simulation were chosen to maximise the upwelling solar irradiance reflected by the surface. The FOV was located in Rome (Latitude: 41°58′ N, Longitude: 12°40′ E), Italy. The acquisition time was assumed midday in July with the solar zenith angle of $\theta_s = 33.97$ and the azimuth solar angle of $\phi_s = 238.41$. The at-nadir viewing angle was chosen to simplify

AMTD
4, 7211–7240, 2011

the view factor calculations for the direct component of radiation reaching the sensor.

3.1 The radiative impact of aerosol loading on the observed radiance

The first analysis was conducted neglecting environmental contribution, or adjacency effect, to the observed radiances. Figure 2 shows the results obtained by simulating the radiance for three values of the aerosol optical thickness, $\tau_{550} = 0.00;1.00;2.00$. The variation in simulated radiance due to increasing aerosol loading was determined for both urban and continental models. Under high surface reflectance, for sand-type FOVs (top images in Fig. 2), the attenuation of radiance, which occurs with the increase in aerosol optical thickness at 550 nm, is more evident for urban (more absorbing) aerosol model than for the continental (less absorbing) model. The spectral behavior associated with the dark surface, water FOVs (bottom images in Fig. 2), was the opposite of the one associated with the bright surfaces. Over dark surfaces observed radiance tends to increase with the increasing of the aerosol loading especially for continental aerosol which are less absorbing than the urban ones.

Results obtained for an idealized hyperspectral instrument, neglecting the adjacency effect, show that the higher sensitivity of the observed radiance for bright surfaces, makes them well suited for aerosol retrievals both in presence of anthropogenic (urban) pollution, or continental-type of aerosols. Dark surfaces, in case of continental aerosols, still provides good condition for retrievals, while in presence of urban aerosols the low radiance sensitivity to variation of the particulate loading make this kind of target non well-suited for inversion.

3.2 The radiative impact of aerosol loading and the environment on the observed radiance

Results obtained in Sect. 3.1 were refined by including environmental contribution (adjacency effect). The analysis of the effect of the 4 possible combinations target-surroundings (Table 2) on the simulated radiance, $L(\lambda)$, was performed by numerical

AMTD
4, 7211–7240, 2011

evaluation of Eq. (2) where $<\rho_{gnd}(\lambda)>$ was calculated off the two surface reflectance spectra presented in Fig. 1. Two of the possible four combination, namely $L^{ss}(\lambda)$ and $L^{ww}(\lambda)$ represent homogeneous situations, while $L^{sw}(\lambda)$ and $L^{ws}(\lambda)$ represent heterogeneous conditions.

3.2.1 Sand

Figure 3 shows the simulation of the sand FOV with $\tau_{550} = 0.0, 1.0, 2.0$ in homogeneous condition (top images), $L^{ss}(\lambda)$, and in the heterogeneous scene (bottom images), $L^{sw}(\lambda)$. The two columns represent the individual results for the urban model (left) and the continental model (right).

Results show that the radiance decreases more rapidly with the increase in the aerosol loading in the urban model than in the continental model. This behavior is more evident for bright targets surrounded by dark areas (lower left image in Fig. 3). While for bright target surrounded by bright environment observed radiance is less sensitive to aerosol load both for continental and urban regimes.

3.2.2 Water

Figure 4 shows the simulation for water FOV with $\tau_{550} = 0.0, 1.0, 2.0$ in the heterogeneous condition (top images), $L^{ws}(\lambda)$, and in homogeneous conditions (bottom images), $L^{ww}(\lambda)$. The two columns represent the individual results for the urban model (left) and the continental model (right).

Plots on left column highlight the spectral regions in which the absorption of the urban aerosol plays a crucial rule in the extinction of the radiation. In these region, mostly in the visible, it is evident that the observed radiance for a dark target is weakly dependent on the aerosol load increase. Therefore even from a simple qualitative analysis it is possible to draw the conclusion that dark targets, in urban aerosolic regimes, represent difficult conditions for aerosol retrievals independently from their surrounding.

AMTD
4, 7211–7240, 2011

Plots on the right column show that variations in the observed radiance are more evident when the dark target is surrounded by dark areas. In this case for $\tau_{550} \in \{0.00, 2.00\}$ the signal at the sensor increases with the increasing of the aerosol load. For dark target in heterogeneous environment (bright surroundings) the variation of the observed radiance is less regular over the same range of $\tau_{550} \in \{0.00, 2.00\}$. Radiances increase rapidly for $0 < \tau_{550} < 1$, while for $\tau_{550} > 1$, dependency on the aerosol load is definitely weaker.

The results obtained from the simulation of the dark surface viewed from the spaceborne sensor, are shown in Fig. 4. The simulated observed radiance indicates the influence of the environment on the observed radiance from water in a homogeneous scene, $L^{ww}(\lambda)$, and a heterogeneous environment composed of a bright surface, $L^{ws}(\lambda)$, as presented in Table 2.

Thus it should be expected that aerosol retrieval using hyperspectral radiance coming from water surface is more sensitive for continental regimes as opposed to the urban ones. Besides, water surface provide a better suited target for retrievals when the FOV is surrounded by dark environment.

4 Specific results for PRISMA-like

In order to evaluate the merits of PRISMA in retrieving aerosol loading specifically for coastal areas composed principally by sand (bright) and dark (water) surface the data used in Sect. 3 were convolved with the first spectrometer response function PRISMA instrument (Table 3) to generate the 92 channels characteristic of this future sensor. The spectral domain was reduced, according to PRISMA specifications, to 400–1000 nm range. While the surface properties, and the aerosol modes were kept identical to those of Sect. 3 (only sand and water targets were considered, in urban and continental regimes), the aerosol loadings were varied at incremental steps of $\Delta\tau_{550} = 0.02$ with the goal to identify, with a quantitative analysis, the conditions and the spectral regions for which the radiance sensitivity to aerosol loading changes is

AMTD
4, 7211–7240, 2011

greater than the specification for the instrument noise (i.e. $\frac{L(\lambda)}{\Delta L(\lambda)} < \mathrm{SNR}$).

4.1 The radiative impact of aerosol loading on the observed radiance

Figure 5 shows the ratio $\frac{L(\lambda)}{\Delta L(\lambda)}$ (in greyscale) for the observed radiances of a PRISMA-like instrument, calculated for aerosol loading $\tau_{550} \in \{0.00, 2.00\}$ with $\Delta\tau_{550} = 0.02$ (on the y-axis) and λ in the range 400–1000 nm (on the x-axis). Results, obtained without taking into account the adjacency effect, show that radiance sensitivity is greater than instrument noise only for urban aerosolic regimes (left column) for both bright and dark targets. For continental regimes (left column), independently on the reflective characteristics of the surface, $\frac{L(\lambda)}{\Delta L(\lambda)}$ was found to be smaller than the SNR only in narrow absorption bands.

Thus, the quantitave analysis proved that, in urban regimes PRISMA would provide observations well suited for optical thickness retrieval especially for $\lambda < 600$ nm independently on the surface reflective properties. In addition retrievals, always in urban regimes, are expected to be more accurate for values of $\tau_{550} < 1.5$ where the instrument sensitivity to changes in the aerosol load is the highest. Continental regimes represent cases where the inversion might require a pre-processing of the observation (such as PCA analysis) to increase the SNR.

4.2 The radiative impact of aerosol and environment on the observed radiance

Results obtained in Sect. 4.1 were refined by including environmental contribution (adjacency effect). The analysis of the effect of the 4 possible combinations target-surroundings (Table 2) on the simulated radiance, $L(\lambda)$, was performed by numerical evaluation of Eq. (2) where $<\rho_{\mathrm{gnd}}(\lambda)>$ was calculated off the two surface reflectance spectra presented in Fig. 1. Two of the possible four combination, namely $L^{\mathrm{ss}}(\lambda)$ and $L^{\mathrm{ww}}(\lambda)$ represent homogeneous situations, while $L^{\mathrm{sw}}(\lambda)$ and $L^{\mathrm{ws}}(\lambda)$ represent heterogeneous conditions.

AMTD
4, 7211–7240, 2011

4.2.1 Sand

Figure 6 shows the ratio $\frac{L(\lambda)}{\Delta L(\lambda)}$ (in greyscale) as function of aerosol loading (y-axis) and wavelength (x-axis) for bright target and bright (top) and dark (bottom) environmental reflectance.

Top images (compared to Fig. 5) show that the adjacency effect for homogeneous conditions do no improve the instrument sensitivity for the continental regime (left column) neither for the urban regime (right column). In case of heterogeneous conditions, both for continental (bottom left) and for the urban (bottom right), the dark environment significantly improves the instrument sensitivity (by reducing the ratio $\frac{L(\lambda)}{\Delta L(\lambda)}$). It is worth mentioning that heterogeneous environment (water surroundings) for bright targets, could improve the accuracy of retrieved aerosol property by enabling inversion algorithms to use more channels (as the spectral range where $\frac{L(\lambda)}{\Delta L(\lambda)} < \text{SNR}$ is broader). Therefore PRISMA-like data are well suited to infer aerosolic properties especially in coastal (heterogeneous) regions, under urban conditions.

4.2.2 Water

Figure 7 shows the ratio $\frac{L(\lambda)}{\Delta L(\lambda)}$ (in greyscale) as function of aerosol loading (y-axis) and wavelength (x-axis) for dark targets and bright (top) and dark (bottom) environmental reflectance. Top images (compared to Fig. 5) show that the adjacency effect for heterogeneous conditions do improve the instrument sensitivity for the continental regime (left column) neither for the urban regime (right column). In case of homogeneous conditions, for continental (bottom left), the dark environment improves the instrument sensitivity (by reducing the ratio $\frac{L(\lambda)}{\Delta L(\lambda)}$) over a broad spectral region. It can be concluded that the sensitivity of the PRISMA-like sensor to the aerosol loading, τ_{550}, in the continental aerosol regime represent optimal retrieval conditions when the target surroundings are dark. For urban aerosol model, the variation of the dependence of radiances on changes in aerosol optical thickness, when viewing a dark surface does

AMTD
4, 7211–7240, 2011

not seem to be well suited for accurate retrievals. Therefore PRISMA observations for continental aerosolic regimes (generally non-anthropogenic) would provide best inversion results when observing dark target (water) in homogenous conditions (water surroundings).

Table 4 summarizes the best viewing conditions for inversion of PRISMA-like data over coastal regions.

5 Conclusions

This study was based on the idea that hyperspectral visible and near infrared data can be used to provide additional and better spectral information on atmospheric aerosol loadings than multispectral sensors currently in orbit. The study, tailored for retrievals over coastal areas, was based on simulated data and was divided in two main parts: a qualitative analysis performed on an idealized hyperspectral instrument; a quantitate analysis performed on a PRISMA-like instrument.

The results of the simulation for idealized instrument, which was performed on surfaces with different reflective characteristics, proved that dark surfaces are ideal to retrieve the properties of aerosols, in coastal areas, especially under continental aerosol regimes. For urban aerosol conditions, aerosol retrieval is expected to be more accurate when the target is a bright surface. These results were derived from the radiative components of the observed radiances. For a dark surface, the fraction of solar incident radiation reflected by the surface is negligible with respect to the component diffused by the aerosol. Under these circumstances for aerosol models characterized by significant absorption (as the urban model), the extinction of the radiation happens to be due to both scattering and absorption, and the individual effect of the scattering is attenuated. Consequently, in presence of absorbing aerosols, as in the urban model, bright surface represent better conditions to retrieve the loading than the dark surface which is characterized by a smaller diffuse component. Furthermore, the sensitivity of the observed radiance to small variation of the optical thickness, for dark FOV surface

AMTD
4, 7211–7240, 2011

increases when those FOVs are surrounded by bright environment heterogenous conditions). On the contrary, the sensitivity is reduced if a bright surface is surrounded by dark environment.

Regarding the PRISMA-like data, the results confirmed that in general this kind of sensors would be well suited for retrievals of τ_{550}. In particular results proved that, over coastal regions, bright surface target (sand) provides, under the urban aerosol model, better conditions for higher retrieval accuracy compared to the continental regimes. Whereas dark surface (water) target are less suitable for aerosol retrieval in urban areas and are better suited with for continental aerosolic regimes. In addition, the analysis of the environmental (surroundings) contribution revealed that for dark target surfaces, the sensitivity of simulated radiance to small variation of optical thickness is enhanced by homogeneous environments as compared to heterogeneous environments. Thus, results showed that adjacency effect, if properly accounted for, improves the sensitivity of the instrument to small variation in aerosol loads, and therefore it might lead to improvements in the retrieval accuracy. Besides the outcome of this study, it is worth emphasizing that the high spatial resolution (Table 3) of PRISMA is expected to enable users to take full advantage of the adjacency effect to improve the accuracy of retrieve aerosol properties, by focusing on optimal situation (homogeneous or heterogeneous targets-surroundings) for any of the two aerosolic regimes (urban, and continental) considered in this study.

Presented findings are expected to have important implications for algorithms dedicated to aerosol retrieval from space-borne remote data. This type of remote data provides a new opportunity to jointly process hyperspectral and high spatial resolution (≈30 m) imagery to achieve improved aerosol detection. Further work is required to establish the merits of PRISMA-like observations to derive aerosol loadings by directly using physically-based inversion algorithm on simulated data or, when available, on real data.

Acknowledgements. We thank the referees for their careful reading and helpful comments that greatly improved the manuscript.

AMTD
4, 7211–7240, 2011

References

Alakian, A., Marion, R., and Briottet, X.: Remote sensing of aerosol plumes: A semi-analytical model, Appl. Optics, 47, 1851–1866, doi:10.1364/AO.47.001851, 2008. 7217

Barnsley, M., Settle, J., Cutter, M., Lobb, D., and Teston, F.: The PROBA/CHRIS mission, a low-cost small satellite for hyperspectral, multi-angle, observations of the earth surface and atmosphere, IEEE Transactions on Geosciences and Remote Sensing, 42, 1512–1520, 2004. 7213

Bassani, C., Cavalli, R. M., and Pignatti, S.: Aerosol optical retrieval and surface reflectance from airborne remote sensing data over land, Sensors, 10, 6421–6438, doi:10.3390/s100706421, 2010. 7214, 7217

d'Almeida, G. A., Koepke, P., and Shettle, E. P.: Atmospheric aerosols: global climatology and radiative characteristics, A. DEEPAK Publishing, Hampton, Virginia, USA, 1991. 7218, 7230

Galeazzi, C., Sacchetti, A., Cisbani, A., and Babini, G.: The PRISMA Program, in: IGARSS 2008: IEEE International Geoscience and Remote Sensing Symposium, 2008, pp. IV – 105 – IV – 108, doi:10.1109/IGARSS.2008.4779667, 2008. 7213, 7219

Gao, B.-C., Montes, M. J., Davis, C. O., and Goetz, A. F. H.: Atmospheric correction algorithms for hyperspectral remote sensing data of land and ocean, Remote Sens. Environ., 113, S17–S24, doi:10.1016/j.rse.2007.12.015, 2009. 7213, 7214

Goetz, A. F. H., Vane, G., Salomon, J. E., and Rock, B. N.: Imaging spectroscopy for Earth remote sensing, Science, 228, 1147–1153, 1985. 7213

Guanter, L., Estellés, V., and Moreno, J.: Spectral calibration and atmospheric correction of ultra-fine spectral and spatial resolution remote sensing data. Application to CASI-1500 data, Remote Sens. Environ., 109, 54–65, doi:10.1016/j.rse.2006.12.005, 2007. 7214, 7217

Guanter, L., Segl, K., and Kaufmann, H.: Simulation of Optical Remote-Sensing Scenes With Application to the EnMAP Hyperspectral Mission, IEEE Transanction on Geoscience and Remote Sensing, 47, 2340–2351, doi:10.1109/TGRS.2008.2011616, 2009. 7213

Holben, B., Eck, T., Slutsker, I., Tanré, D., Buis, J., Setzer, A., Vermote, E., Reagan, J., Kaufman, Y., Nakajima, T., Lavenu, F., Jankowiak, I., and Smirnov, A.: AERONET – A federated instrument network and data archive for aerosol characterization, Remote Sens. Environ., 66, 1–16, doi:10.1016/S0034-4257(98)00031-5, 1998. 7217

IPCC: The Scientific Basis. IPCC Third Assessment Report: Climate Change 2001 (TAR), Tech. rep., Intergovernmental Panel on Climate Change, edited by: Houghton, J. T., Ding, Y.,

AMTD
4, 7211–7240, 2011

Griggs, D. J., Noguer, N., van der Linden, P. J., Xiaosu, D., Maskell, K., and Johnson, C. A., 2001. 7212

IPCC: The Physical Science Basis. IPCC Fourth Assessment Report: Climate Change 2007 (AR4), Tech. rep., Intergovernmental Panel on Climate Change, edited by: Solomon, S., Qin, D., Manning, M., Chen, Z., Marquis, M., Averyt, K. B., Tignor, M., and Miller, H. L., 2007. 7212

Kaufman, Y. J., Tanré, D., Gordon, H. R., Nakajima, T., Lenoble, J., Frouin, R., Grassl, H., Herman, B. M., King, M., and Teillet, P. M.: Operational remote sensing of tropospheric aerosol over land from EOS moderate resolution imaging spectroradiometer, J. Geophys. Res., 102, 17051–17067, doi:10.1029/96JD03988, 1997a. 7214

Kaufman, Y. J., Tanré, D., Gordon, H. R., Nakajima, T., Lenoble, J., Frouin, R., Grassl, H., Herman, B. M., King, M., and Teillet, P. M.: Passive remote sensing of tropospheric aerosol and atmospheric correction for aerosol effect, J. Geophys. Res., 102, 16815–16830, doi:10.1029/97JD01496, 1997b. 7217

Kaufman, Y. J., Wald, A., Remer, L. A., Gao, B.-C., Li, R. R., and Flynn, L.: The MODIS 2.1 µm channel-correlation with visible reflectance for use in remote sensing of aerosol, IEEE Transanction on Geoscience and Remote Sensing, 35, 1286–1298, doi:10.1109/36.628795, 1997c. 7213

Kaufman, Y. J., Gobron, N., Pinty, B., Widlowski, J.-L., and Verstraete, M. M.: Relationship between surface reflectance in the visible and mid-IR used in MODIS aerosol algorithm – theory, Geophys. Res. Lett., 29, 31–1–31–4, doi:10.1029/2001GL014492, 2002. 7213

Kaufmann, H., Segl, K., Guanter, L., Hofer, S., Foerster, K.-P., Stuffler, T., Mueller, A., Richter, R., Bach, H., Hostert, P., and Chlebek, C.: Environmental Mapping and Analysis Program (EnMAP) – Recent Advances and Status, in: IGARSS 2008: IEEE International Geoscience and Remote Sensing Symposium, 2008, pp. IV – 109 – IV – 112, doi:10.1109/IGARSS.2008.4779668, 2008. 7213

King, M., Kaufman, Y., Tanré, D., and Nakajima, T.: Remote sensing of tropospheric aerosols from space: Past, present, and future, B. Am. Meteorol. Soc., 88, 2229–2259, doi:10.1175/1520-0477(1999)080<2229:RSOTAF>2.0.CO;2, 1999. 7213

Kokhanovsky, A. A.: Aerosol optics: light absorption and scattering by particles in the atmosphere, Praxis Publishing Ltd, Chichester, UK, 2008. 7216, 7218, 7230

Kokhanovsky, A. A., Breon, F.-M., Cacciari, A., Carboni, E., Diner, D., Nicolantonio, W. D., Grainger, R. G., Grey, W. M. F., Höller, R., Lee, K.-H., Li, Z., North, P. R. J., Sayer, A. M.,

AMTD
4, 7211–7240, 2011

Thomas, G. E., and von Hoyningen-Huene, W.: Aerosol remote sensing over land: a comparison of satellite retrievals using different algorithms and instruments, Atmos. Res., 85, 372–394, doi:10.1016/j.atmosres.2007.02.008, 2007. 7213

Kokhanovsky, A. A., Deuzé, J. L., Diner, D. J., Dubovik, O., Ducos, F., Emde, C., Garay, M. J., Grainger, R. G., Heckel, A., Herman, M., Katsev, I. L., Keller, J., Levy, R., North, P. R. J., Prikhach, A. S., Rozanov, V. V., Sayer, A. M., Ota, Y., Tanré, D., Thomas, G. E., and Zege, E. P.: The inter-comparison of major satellite aerosol retrieval algorithms using simulated intensity and polarization characteristics of reflected light, Atmos. Meas. Tech., 3, 909–932, doi:10.5194/amt-3-909-2010, 2010. 7214

Kotchenova, S. Y., Vermote, E. F., Levy, R., and Lyapustin, A.: Radiative transfer codes for atmospheric correction and aerosol retrieval: Intercomparison study, Appl. Optics, 47, 2215–2226, doi:10.1364/AO.47.002215, 2008. 7214, 7216

Lenoble, J.: Radiative Transfer in scattering and absorbing atmospheres: standard computational procedures, A. DEEPAK Publishing, Hampton, Virginia, USA, 1985. 7218, 7230

Vermote, E. F. and Kotchenova, S.: Atmospheric correction for the monitoring of land surfaces, J. Geophys. Res., 113, 675–686, doi:10.1109/36.581987, 2009. 7216

Vermote, E. F., Tanré, D., Deuzé, J. L., Herman, M., and Morcrette, J. J.: Second simulation of the satellite signal in the solar spectrum, 6S: An overview, IEEE Transactions on Geoscience and Remote Sensing, 35, 675–686, doi:10.1109/36.581987, 1997. 7214, 7216

Vermote, E. F., Tanré, D., Deuzé, Herman, M., Morcrette, J. J., and Kotchenova, S. Y.: Second Simulation of a Satellite Signal in the Solar Spectrum – Vector (6SV), http://6s.ltdri.org, 6S User Guide Version 3, 2006. 7214, 7218, 7230

AMTD
4, 7211–7240, 2011

Table 1. The volumetric percentage of the four basic components (sea-salt, water-soluble, soot and dust-like) describing the urban and continental aerosol model (Lenoble, 1985; d'Almeida et al., 1991; Vermote et al., 2006; Kokhanovsky, 2008).

	Water-soluble	Soot	Dust-like	Oceanic
Urban	61 %	22 %	17 %	0 %
Continental	29 %	1 %	70 %	0 %

AMTD
4, 7211–7240, 2011

Table 2. The observed radiance simulated using sand and water for viewed and adjacent targets.

Observed radiance	Viewed target	Adiacent targets
$L^{ss}(\lambda)$	sand	sand
$L^{sw}(\lambda)$	sand	clear-water
$L^{ww}(\lambda)$	clear-water	clear-water
$L^{ws}(\lambda)$	clear-water	sand

AMTD
4, 7211–7240, 2011

Table 3. PRISMA instrument specifications.

Parameter	I Spectrometer VNIR	II Spectrometer SWIR
Spectral range	400–1000 nm	920–2505
Spectral resolution (FWHM)	≤10 nm	≤12 nm
Spectral bands	92	171
Swath width (km)	30	30
Ground sample distance (m)	30	30
SNR (Signal-to-Noise Ratio)	≥200 in the range 0.4–1.0 µm 600 @ 0.65 µm	≥200 in the range 1.00–1.75 µm >400 @ 1.55 µm ≥100 in the range 1.95–2.35 µm >200 @ 2.1 µm

AMTD
4, 7211–7240, 2011

Table 4. Condition for accurate aerosol retrieval via PRISMA-like data in coastal areas.

Aerosol model	Viewed target	Environment
Urban	Sand	Water
Continental	Water	Water

AMTD
4, 7211–7240, 2011

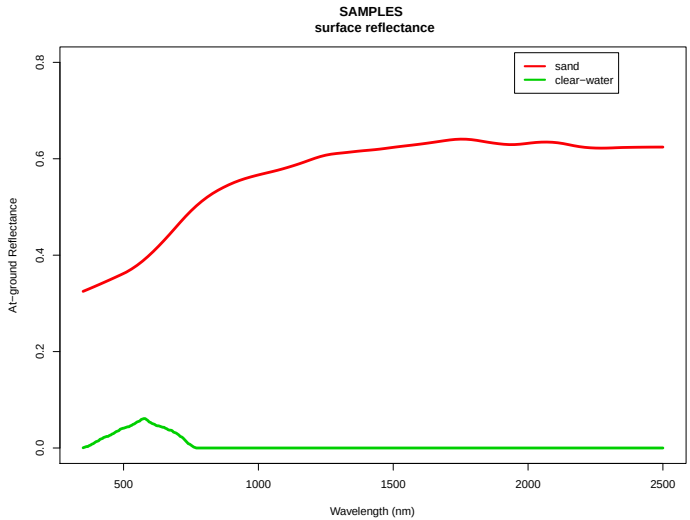

Fig. 1. Surface reflectance, $\rho_{gnd}(\lambda)$ contained in the 6SV1 source code: sand for bright and water for dark in the spectral domain: 400–2500 nm sampled at 2.5 nm.

AMTD
4, 7211–7240, 2011

Influence of aerosol and surface reflectance variability on radiance

C. Bassani et al.

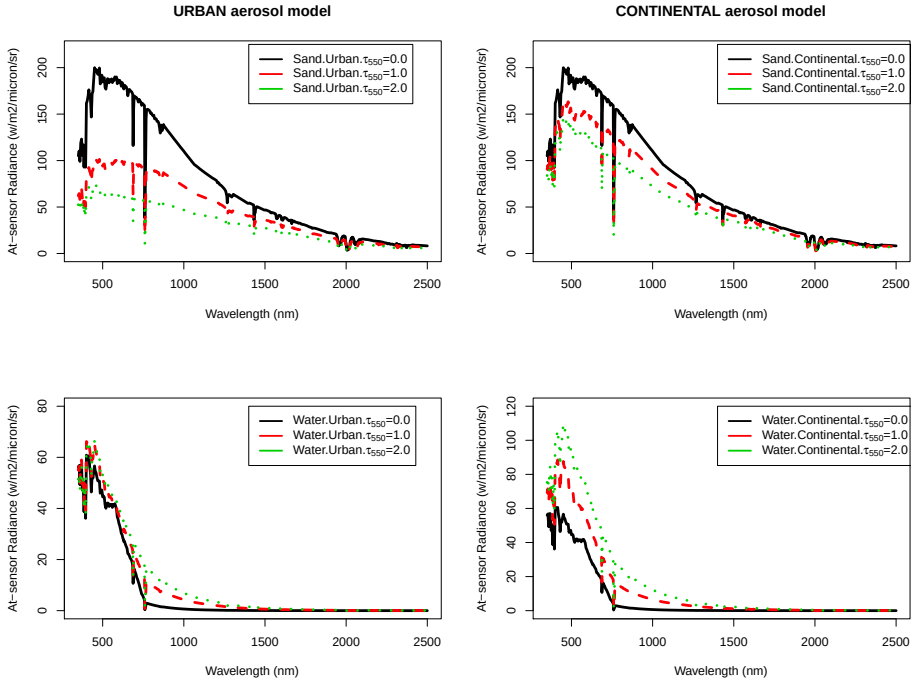

Fig. 2. Nadir observed radiance (At-sensor radiance in the plots) with $\tau_{550} = 0.0, 1.0, 2.0$ using the urban (left column) and continental (right column) aerosol model for sand (first row) and water (second row).

AMTD
4, 7211–7240, 2011

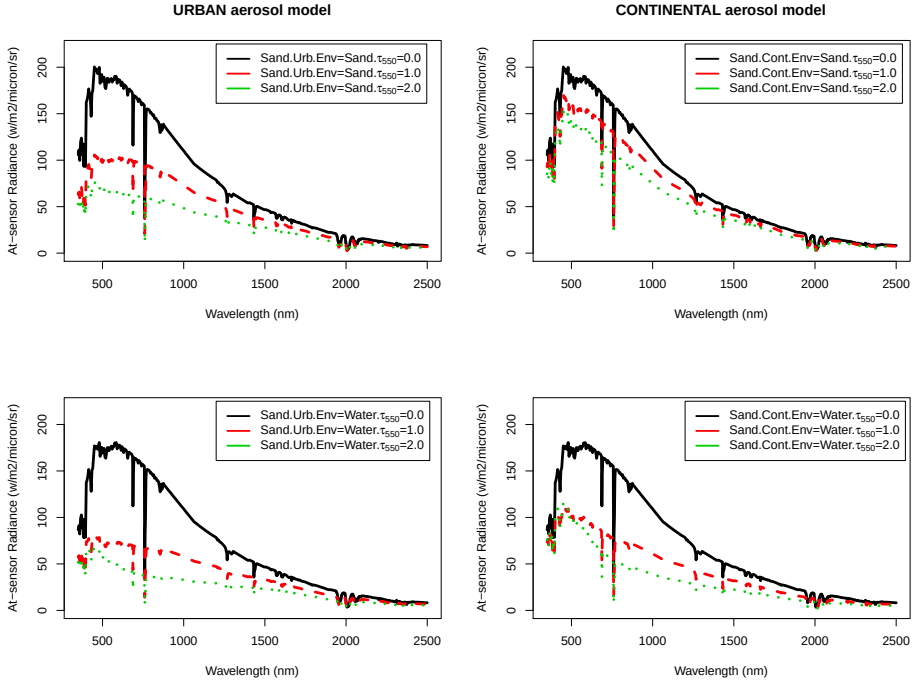

Fig. 3. Nadir observed radiance (At-sensor radiance in the plots) with $\tau_{550} = 0.0, 1.0, 2.0$ using the urban (first column) and continental (second column) aerosol models to view sand surrounded by sand, $L^{ss}(\lambda)$ (first row) and water, $L^{sw}(\lambda)$ (second row).

AMTD
4, 7211–7240, 2011

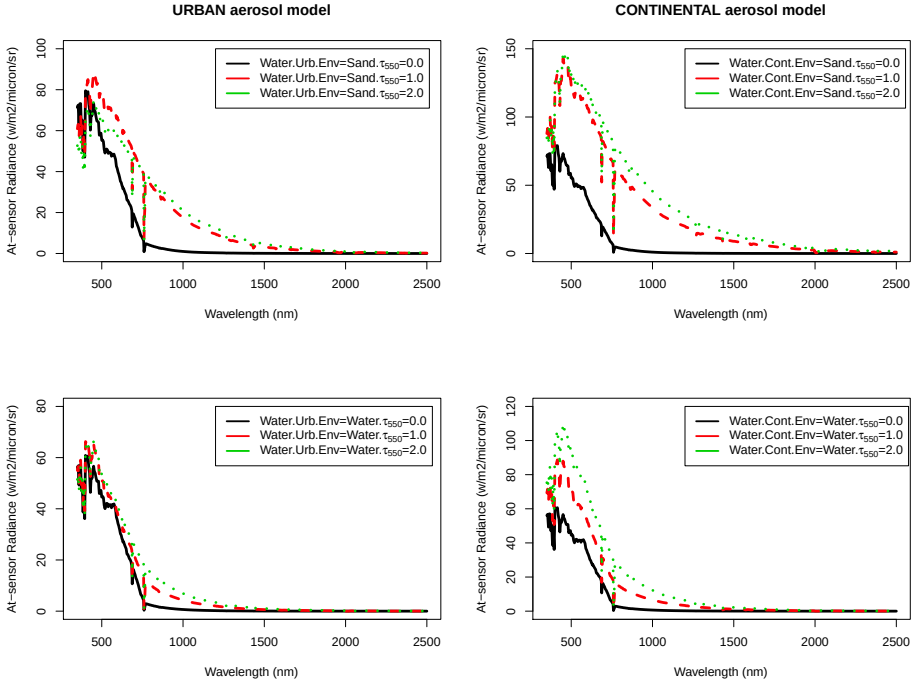

Fig. 4. Nadir observed radiance (At-sensor radiance in the plots) with $\tau_{550} = 0.0, 1.0, 2.0$ using the continental and urban aerosol models to view water surrounded by sand, $L^{ws}(\lambda)$ and water, $L^{ww}(\lambda)$.

AMTD
4, 7211–7240, 2011

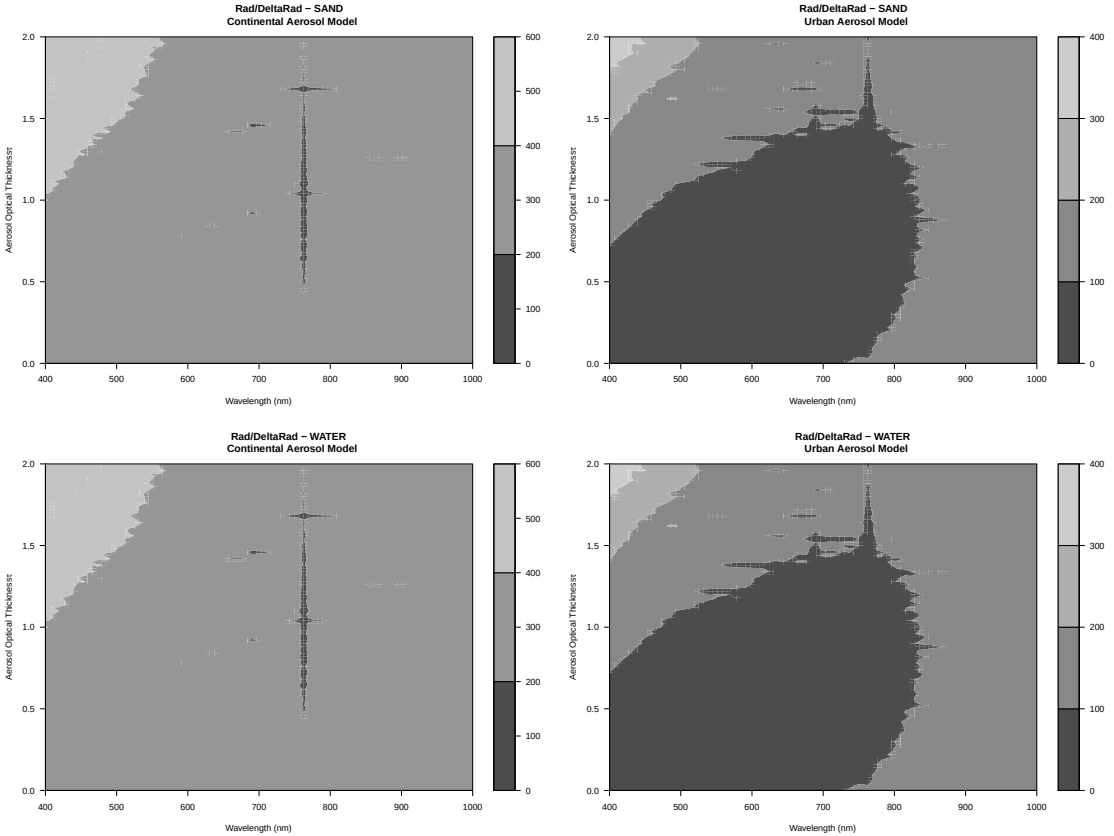

Fig. 5. The $\frac{L(\lambda)}{\Delta L(\lambda)}$ in the PRISMA observed radiance simulated by increasing the aerosol loading, $\tau_{550} \in \{0.00 - 2.00\}$ with $\Delta\tau_{550} = 0.02$, for sand (first row) and water (second row) in continental (first column) and urban (second column) aerosol model.

AMTD
4, 7211–7240, 2011

Influence of aerosol and surface reflectance variability on radiance

C. Bassani et al.

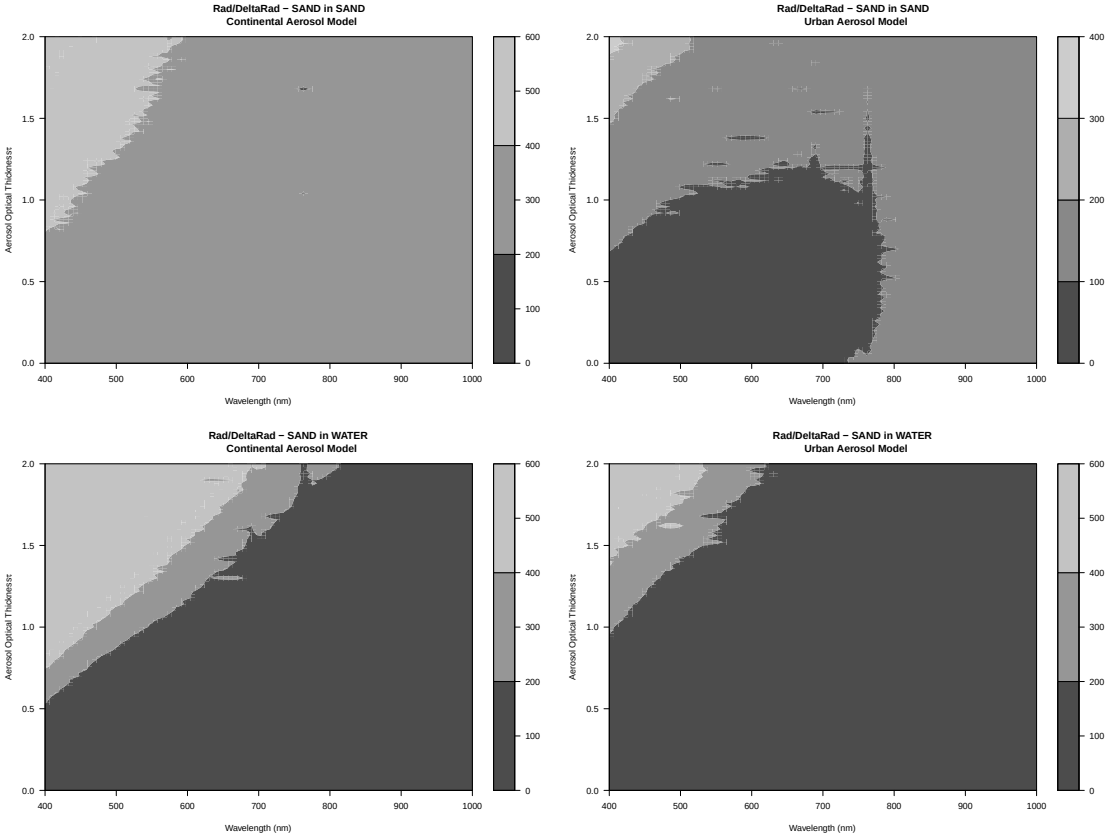

Fig. 6. The $\frac{L(\lambda)}{\Delta L(\lambda)}$ in the PRISMA observed radiance simulated by increasing the aerosol loading, $\tau_{550} \in \{0.00 - 2.00\}$ with $\Delta\tau_{550} = 0.02$, for the sand surface given the environmental contribution of sand (first row) and water (second row) under continental (first column) and urban (second column) aerosol model.

AMTD
4, 7211–7240, 2011

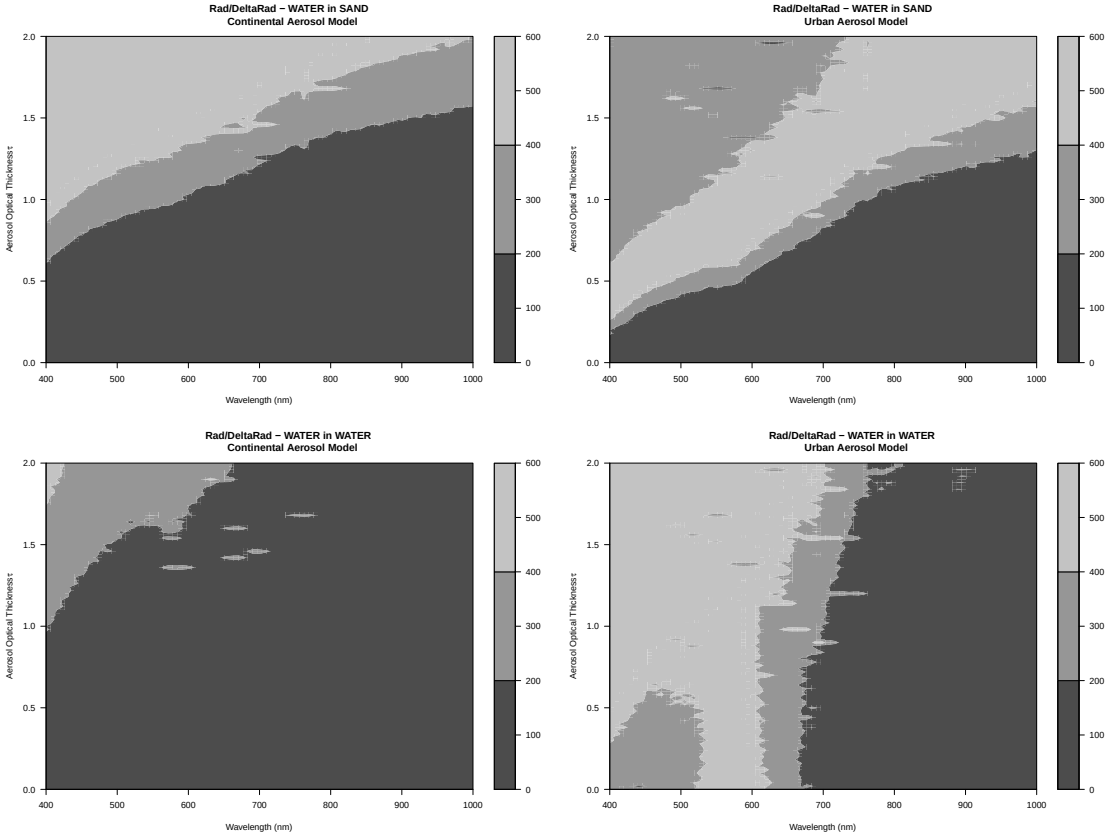

Fig. 7. The $\frac{L(\lambda)}{\Delta L(\lambda)}$ in the PRISMA observed radiance simulated by increasing the aerosol loading, $\tau_{550} \in \{0.00 - 2.00\}$ with $\Delta\tau_{550} = 0.02$, for water surrounded by sand (first row) and water (second row) under continental (first column) and urban (second column) aerosol model.

AMTD
4, 7211–7240, 2011

Influence of aerosol and surface reflectance variability on radiance

C. Bassani et al.